Receiver Design for a Bionic Nervous System: Modeling the Dendritic Processing Power

Angela Sara Cacciapuoti, *Member, IEEE*, and Marcello Caleffi, *Member, IEEE*

***Abstract*—Intrabody nanonetworks for nervous system monitoring are envisioned as a key application of the Internet of Nano-Things (IoNT) paradigm, with the aim of developing radically new medical diagnosis and treatment techniques. Indeed, very recently, bionic devices have been implanted inside a living human brain as innovative treatment for drug-resistant epilepsy. In this context, this paper proposes a systems-theoretic communication model to capture the actual behavior of biological neurons. Specifically, biological neurons exhibit physical extension due to their projections called dendrites, which propagate the electrochemical stimulation received via synapses to the soma. Experimental evidences show that the dendrites exhibit two main features: 1) the compartmentalization at the level of the dendritic branches of the neuronal processes and 2) the location-dependent preference for different frequencies. Stemming from these experimental evidences, we propose to model the dendritic tree as a spatiotemporal filter bank, where each filter models the behavior in both space and time of a dendritic branch. Each filter is fully characterized along with the overall neuronal response. Furthermore, sufficient conditions on the incoming stimulus for inducing a null-neuronal response are derived. The conducted theoretical analysis shows that: 1) the neuronal information is encoded in the stimulus temporal pattern, i.e., it is possible to select the neuron to affect by changing the stimulus frequency content; in this sense, the communication among neurons is frequency-selective and 2) the spatial distribution of the dendrites affects the neuronal response; in this sense, the communication among neurons is spatial-selective. The theoretical analysis is validated through a real neuron morphology.**

***Index Terms*—Dendritic tree, Internet of Nano-Things (IoNT), intrabody networks, nanonetworks, receiver, spatial-frequency selectivity.**

I. Introduction

In THE last years, the *Internet of NanoThings* (IoNT) has been proposed as a novel network paradigm aiming at interconnecting nanoscale devices, referred to as *nanomachines*, with classical networks and ultimately the Internet [1]. *Intrabody nanonetworks*, in which nanomachines are deployed inside the human body and remotely controlled from the macroscale and over the Internet by an external user such as a healthcare provider, are envisioned as the ideal candidate for applying the IoNT paradigm to develop radically new medical diagnosis and treatment techniques [1], [2]. Indeed, very recently, intrabody nanonetworks have been proposed for human nervous system monitoring [3]–[6] by exploiting the dimensional similarity of the nanomachines with the nervous biological structures, and machines have been already implanted inside a living human brain as innovative treatment for drug-resistant epilepsy [7].

Despite the aforementioned breakthroughs, several questions and challenges must be addressed to design a fully functional intrabody nanonetwork deployed inside the nervous system. To this aim, the first step is to study the physiological mechanisms underlying the neuronal activities with an engineering abstraction and to map such mechanisms into communication engineering system models [4]. In fact, only if such a mapping is available, it may be possible to understand how to control the artificial nanomachines deployed inside the nervous system. Hence, the aforementioned mapping has been a subject of study in the latest years.

In literature, the widely adopted communication model for describing the neuron mechanisms is the so-called point neuron model, according to which a neuron is point-wise without physical extension. Consequently, a targeted neuron, referred to as *postsynaptic neuron*, mainly acts either as a single low-pass filter [8], by temporally integrating the incoming stimuli generated by the surrounding neurons, referred to as presynaptic neurons, or as a single bandpass filter [4], centered on a certain frequency, called resonance frequency.

However, biological neurons are not point-like. Indeed, as shown in Fig. 1, they are constituted by physical projections, called *dendrites*, which propagate the electrochemical stimulation received via synapses to the cell body or soma. In particular, evidences from experimental studies have shown that the dendritic morphology is one of the crucial factors determining how signals coming from individual synapses are processed [9]. A clear fact supporting this statement is that several neuropathological conditions are characterized by abnormalities in dendritic tree structure, including some retardation syndromes [10] and neurodegenerative diseases [11].

As a consequence, an effective neuron communication model should take into account the complex physical structure of a neuron. More in detail, a growing body of experimental evidence shows a high compartmentalization at the level of individual dendritic branches of many electrical, biochemical, and cellular processes, fundamental to the neuron physiology [12]–[15]. According to these evidences, the dendrites act as independent processing and signaling units, referred in the

Manuscript received February 12, 2015; revised April 13, 2015; accepted May 14, 2015. Date of publication June 01, 2015; date of current version January 20, 2016. This work was supported in part by the Italian PON projects "SIRIO: Servizi per l'Infrastruttura di Rete wIreless Oltre il 3G" and "FERSAT: studio di un sistema di segnalamento FERroviario basato sullinnovativo utilizzo delle tecnologie SATellitari e della loro integrazione con le tecnologie terrestri" and in part by the Campania POR project myOpenGov.

The authors are with the DIETI Department, University of Naples Federico II, Naples I-80125, Italy (e-mail: angelasara.cacciapuoti@unina.it; marcello.caleffi@unina.it).

Digital Object Identifier 10.1109/JIOT.2015.2438098

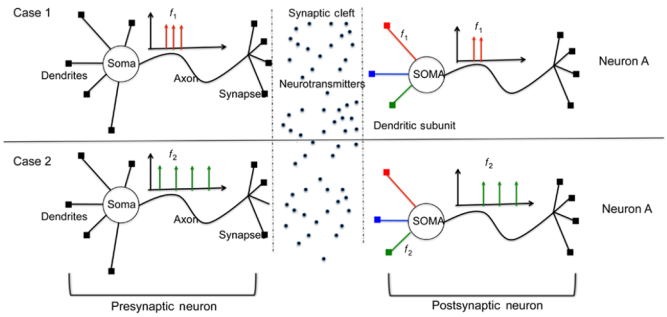

Fig. 1. Location-dependent frequency filtering. Case 1: An incoming stimulus with interspike frequency f_1 activates only the dendritic subunit, denoted with the red color of the postsynaptic neuron A. Case 2: An incoming stimulus with interspike frequency f_2 activates only the dendritic subunit, denoted with the green color of the postsynaptic neuron A.

following to as *dendritic subunits*.[1] Each subunit performs local processing, whose output is broadcasted within the neuron or to different neurons via dendritic transmission and neuromodulator release [12]–[14]. The processing specificity of each dendritic subunit is driven by and reflects the complex dendritic branching, tapering, and the nonuniform ion-channel distribution [16] that make the electrical properties of a neuron not uniform within the dendritic tree.

Very recently in [15], it has been shown that the compartmentalization of the dendritic processing causes a crucial phenomenon: different dendritic subunits express different frequency preferences, i.e., the maximum in their frequency response changes in the space. Let us describe this concept with the example depicted in Fig. 1, where the postsynaptic neuron A exhibits three different dendritic subunits characterized by frequency preferences at f_1, f_2, and f_3, respectively. In Case 1, the presynaptic neuron generates electrical pulses, referred to as *action potentials* (APs) or spikes, with a period corresponding to the frequency f_1. Hence, the dendritic subunit of neuron A activated by the incoming stimulus is the one labeled with the red color, since its frequency response has a maximum at f_1. In Case 2, the presynaptic neuron generates spikes with an interspike frequency equal to f_2. Hence, the dendritic subunit of neuron A activated by the incoming stimulus is now the one labeled with the green color. As a consequence, a stimulus may or not elicit a spike depending on its timing and on the dendritic subunit frequency preference.

In this paper, a communication engineering model is designed for capturing the behavior of biological neurons, by accounting for both the peculiar features of the dendritic biophysics: 1) the compartmentalization at the level of the dendritic subunits of the neuronal processes and 2) the location-dependent preference for different frequencies. To the best of our knowledge, this is the first work that addresses this key issue.

Specifically, we propose to model the dendritic tree of a neuron as a *receiver spatiotemporal filter bank*, where each filter models the behavior in both space and time of a dendritic subunit. To capture the trial-to-trial variability of the neuronal responses, we conduct the analysis through a stochastic approach. In particular, we first characterize the input–output relationship of each dendritic subunit, with the aim of mapping its biophysics in a communication system model. More in detail, we derive: 1) the attenuation and the delay experienced by a stimulus at an arbitrary location of an arbitrary dendritic subunit; 2) the neuron firing probability, i.e., the probability of a neuron to generate APs, due to the activation of an arbitrary dendritic subunit at an arbitrary location; 3) the sufficient conditions for an input stimulus to induce a null neuronal response; and 4) the bandwidth characterization of the filter modeling a dendritic subunit as a function of both the dendritic subunit impedance and its spatial distribution. Then, we characterize the overall neuronal response by generalizing the above analysis. Finally, the theoretical analysis is validated through numerical simulation, using an experimentally reconstructed morphology of a multipolar rat neuron.

This paper is organized as follows. In Section II, we describe the biophysics of the dendritic tree. In Section III, we develop a receiver design for capturing the actual neuron behavior, and we derive the above-mentioned results. In Section IV, we validate the theoretical analysis with a real neuron morphology through numerical simulations. In Section V, we discuss the derived results by providing insights on the design of future IoNT applications. Finally, Section VI concludes this paper, and some proofs are gathered in the Appendix.

II. Biophysics of Dendrites

Dendrites are the branched projections of a neuron. They are the largest component in both surface area and volume of the brain and their specific morphology is used to classify neurons into classes: pyramidal, Purkinje, amacrine, stellate, etc. Hence, different types of neurons exhibit distinctive and characteristic dendrite branching patterns. Dendrites propagate the electrochemical stimulation received via synapses, which are located at various points throughout the dendritic tree, to the cell body or soma. Consequently, they play a central role in neural computation [9]. A typical dendritic tree receives approximately 10 000 synaptic inputs distributed over the dendritic surface. When activated, each of these inputs produces a local conductance change for specific ions at the postsynaptic membrane, followed by a flow of the corresponding ion current between the two sides of the postsynaptic membrane. As a result, a local change in membrane potential is generated and spread along the dendritic branches [17]. This spread depends on the morphology of the tree, on the electric properties of its membrane and cytoplasm. Specifically, the various synaptic inputs that are distributed over the dendritic tree interact in time and in space by determining the input–output properties of the neuron.

As mentioned in Section I, a growing body of experimental evidence shows a highly compartmentalization at the level of individual dendritic branches of many electrical, biochemical, and cellular processes, fundamental to the neuron physiology [12]–[15]. According to these evidences, the dendrites act as independent processing and signaling units, performing local computations that are then broadcast to the rest of the neuron, or to other neurons via dendritic transmission and neuromodulator release. The specificity of the dendritic subunit processing

[1]For a formal definition of dendritic subunit, refer to Section III.

is driven by and reflects the complex dendritic branching, tapering, and the nonuniform ion-channel distribution on the dendrites [16] that make the electrical properties of a neuron not uniform within the dendritic tree. This highly compartmentalization induces different dendrites to express different frequency behaviors, i.e., to express different frequency preferences [15].

Several experiments *in vivo* have directly measured the input–output relationship of dendrites using continuous-time current injection [18]. These studies reveal that the dendritic transmission of time-varying signals is characterized by a linear input–output relationship. This finding is remarkable since dendrites have a full complement of nonlinear voltage-dependent channels, as aforementioned. Regarding their frequency behavior, until recently, experimental methods did not allow direct studies of dendrites, and their frequency response was supposed to be governed only by a low-pass behavior [18]. However, many experiments [19]–[21] show that biological neurons can exhibit a bandpass behavior centered on a frequency, called resonance frequency, whose value depends on the biophysical parameters affecting the resting state of the membrane, e.g., the membrane leak conductance and the potassium channel density. Stemming from these recent findings, in the next section, we propose a systems-theoretic communication engineering model for capturing the actual neuronal behavior, by accounting for the complex dendritic biophysics.

III. Receiver Design: Systems-Theoretic Model

In this section, we propose a systems-theoretic communication model to capture the complex neuronal behavior, by accounting for both the peculiar features of the dendritic biophysics: 1) the compartmentalization at the level of individual dendritic branches of the neuronal processes and 2) the location-dependent preference for different frequencies. These features are a consequence of the aforementioned complex dendritic branching, tapering, and the nonuniform spatial distribution of the ionic channels on the dendrites, which make the electrical properties of a neuron be not uniform within the dendritic tree. Preliminarily, we give the definition of dendritic subunit [12]–[14], which will be used through the paper.

Definition 1: A dendritic subunit denotes an electrically homogeneous region within the dendritic tree.

As described in Section II, each dendritic subunit acts as separate functional block. This phenomenon along with the location-dependent preference for certain frequencies led us to propose the systems-theoretic communication model shown in Fig. 2. According to this model, a neuron is modeled as spatiotemporal filter bank, where each dendritic subunit within the dendritic tree acts as a distinct filter, exhibiting different frequency preferences.[2] The number and the dimensions of the dendritic subunits depend on the neuron characteristics [12]–[14]. In the following, without loss of generality, we denote with $\mathcal{D} \triangleq \{1, 2, \ldots, D\}$ the set of distinct dendritic subunits, whose cardinality is $|\mathcal{D}| = D$.

[2]As described in Section II, the frequency behavior of a dendritic subunit is mainly either low-pass or bandpass.

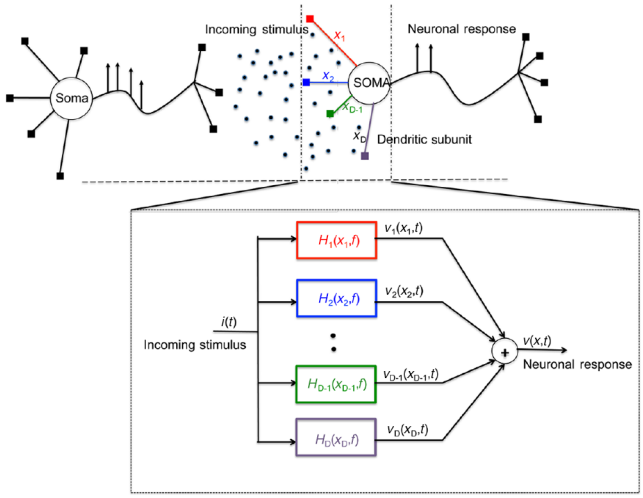

Fig. 2. Spatiotemporal filter bank: one-to-one mapping between dendritic biophysics and receiver block.

A. Dendritic Subunit Response

Definition 2: $H_i(x_i, f)$ denotes the spatial-frequency response of the filter modeling the ith dendritic subunit, with x_i denoting the distance between the application point of the stimulus on the ith dendritic subunit and the spike-initiation zone near the soma [15], [19]. Its inverse Fourier transform (FT) is denoted with $h_i(x_i, t)$.

Since, in neuroscience, the membrane impedance model of dendrites [18], [19], [22] has been shown to provide a near-perfect fit to the dendrite-to-soma input–output relationship for the main trunk, in the following, we adopt such linear model to characterize each $H_i(x_i, f)$. Specifically, by denoting with $Z_i(f)$ and $Z_{a,i}(f)$ the dendritic membrane impedance and the impedance of the intracellular cytoplasm, respectively, the generalized cable equation in the Fourier domain is [19], [22]

$$\frac{\partial^2 V(x_i, f)}{\partial x_i^2} = \gamma_i^2(f) V(x_i, f) \tag{1}$$

where $V(x_i, f)$ is the FT of the voltage response and $\gamma_i(f)$ is the frequency-dependent propagation constant

$$\gamma_i^2(f) \triangleq \frac{Z_{a,i}(f)}{Z_i(f)}. \tag{2}$$

$Z_{a,i}(f)$ is usually an ohmic resistance, i.e., $Z_{a,i}(f) = r_{a,i}$. Moreover, the nature of the dendritic membrane is fully contained in $\gamma_i(f)$ and does not affect the form of (1). The solution of (1) when a δ-current impulse is injected at the origin and the voltage is recorded at a distance x_i farther away, subject to the boundary condition that $V(x_i, f)$ goes to zero as $x_i \to \infty$, is the spatial-frequency response $H_i(x_i, f)$

$$H_i(x_i, f) = \frac{1}{2} \frac{r_{a,i}}{\gamma_i(f)} e^{-x_i \gamma_i(f)}. \tag{3}$$

By recording the voltage at the origin, and by accounting for (2), the input impedance of the dendritic subunit is obtained

$$H_i(0, f) = \frac{1}{2} \frac{r_{a,i}}{\gamma_i(f)} = \frac{1}{2} \sqrt{Z_i(f) r_{a,i}}. \tag{4}$$

Hence, (3) can be rewritten as follows:

$$H_i(x_i, f) = H_i(0, f)e^{-x_i\gamma_i(f)}. \tag{5}$$

Remark 1: From (4), it follows that the frequency behavior of the input impedance $H_i(0, f)$ coincides with the one of the dendritic membrane impedance $Z_i(f)$. Hence, if the dendritic membrane is resonant, i.e., $Z_i(f)$ exhibits a bandpass behavior, so does $H_i(0, f)$ and vice versa. The same consideration holds if $Z_i(f)$ exhibits a low-pass behavior. In particular, the frequency maximizing the amplitude response of $H_i(0, f)$ coincides with the one maximizing the amplitude response of $Z_i(f)$. This agrees with the results in [19].

Remark 2: From (5), by reasoning as in [19], it follows that the frequency behavior of the spatial-frequency response $H_i(x_i, f)$ coincides for any x_i with the one of $Z_i(f)$. Hence, if $Z_i(f)$ exhibits a bandpass/low-pass behavior, so does $H_i(x_i, f)$ (the converse does not hold). However, the frequency assuring the maximum amplitude response of $H_i(x_i, f)$ does not coincide necessarily with the one maximizing the amplitude response of $Z_i(f)$. In particular, from (5), it results that the frequency behavior of $H_i(x_i, f)$ can be modified by varying either $Z_i(f)$ (for instance, by varying the density of the voltage-gated ion channels) or the application point of the stimulus on the dendritic subunit through x_i.

1) Attenuation and Delay Expressions: The attenuation and delay experienced by a stimulus through the dendritic subunit when the stimulus is applied at a x_i distance far away from the soma are analytically derived through the spatial–frequency response expressed in (5). The attenuation $\Lambda_i(x_i, f)$, as function of the frequency f and the distance x_i, is computed as the inverse of the absolute value of $H_i(x_i, f)$. Hence, by accounting for (5) and (4), $\Lambda_i(x_i, f)$ is given by

$$\Lambda_i(x_i, f) \triangleq \frac{1}{|H_i(x_i, f)|} = \frac{e^{x_i\mathrm{Re}(\gamma_i(f))}}{|H_i(0, f)|} = \frac{2\, e^{x_i\mathrm{Re}(\gamma_i(f))}}{\left|\sqrt{Z_i(f) r_{a,i}}\right|}. \tag{6}$$

By evaluating the square root of a complex function and by accounting for (2), (6) is rewritten as follows:

$$\Lambda_i(x_i, f) = \frac{2\, e^{x_i\sqrt{\frac{r_{a,i}}{|Z_i(f)|}}\cos\left(\frac{\angle Z_i(f)}{2}\right)}}{\sqrt{|Z_i(f)|\, r_{a,i}}}. \tag{7}$$

In (7), $\beta_i(f) \triangleq \frac{1}{\mathrm{Re}(\gamma_i(f))} = \left(\sqrt{\frac{r_{a,i}}{|Z_i(f)|}}\cos\left(\frac{\angle Z_i(f)}{2}\right)\right)^{-1}$ is the *generalized frequency-dependent space constant*, which represents the distance over which a sinusoidal voltage of frequency f decays to $1/e$ of its original value [19], [22], and it measures the electrical compactness of the dendritic subunit.

Remark 3: From (6), it follows that the attenuation $\Lambda_i(x_i, f)$ increases exponentially with x_i, and it achieves its minimum value in correspondence of the frequency maximizing the amplitude response of $H_i(x_i, f)$, as expected.

The delay $\Delta_i(x_i, f)$, as function of the frequency f and the distance x_i, is computed as the frequency first derivative of the phase of $H_i(x_i, f)$. By accounting for (5) and (4), and by denoting with $\eta_i(f) \triangleq \mathrm{Im}(\gamma_i(f)) = -\sqrt{\frac{r_{a,i}}{|Z_i(f)|}}\sin\left(\frac{\angle Z_i(f)}{2}\right)$, the phase has the following expression:

$$\begin{aligned}\angle H_i(x_i, f) &= -\frac{r_{a,i}}{2}\tan^{-1}\frac{\mathrm{Im}(\gamma_i(f))}{\mathrm{Re}(\gamma_i(f))} - x_i\mathrm{Im}(\gamma_i(f)) \\ &\triangleq -\frac{r_{a,i}}{2}\tan^{-1}\left(\eta_i(f)\beta_i(f)\right) - x_i\,\eta_i(f).\end{aligned} \tag{8}$$

Hence, the delay $\Delta_i(x_i, f)$ is given by

$$\begin{aligned}\Delta_i(x_i, f) &\triangleq -\frac{d\angle H_i(x_i, f)}{df} \\ &= \frac{r_{a,i}}{2\left(1+\tan^2\left(\frac{\angle Z_i(f)}{2}\right)\right)} \\ &\quad\times\left(\frac{d\eta_i(f)}{df}\beta_i(f) + \eta_i(f)\frac{d\beta_i(f)}{df}\right) + x_i\frac{d\eta_i(f)}{df}.\end{aligned} \tag{9}$$

Remark 4: From (9), it follows that the delay $\Delta_i(x_i, f)$ increases linearly with x_i.

2) Dendritic Subunit Firing Probability: Since the incoming stimulus on a targeted neuron depends on the state of the presynaptic neuron which in turn depends on the background synaptic input converging on the presynaptic neuron and on the action of neuromodulators, a stochastic approach is required for modeling the input current. It has been widely shown that a nonhomogeneous Poisson impulse process is able to effectively describe the neuron trial-to-trial variability [8], [15]. Hence, we model the input current to the considered targeted neuron according to this stochastic process

$$i(t) = \sum_{i=1}^{N(t)}\delta(t - t_i) \tag{10}$$

where $N(t)$ is a nonhomogeneous Poisson process whose rate $\lambda(t)$ is a function of the time, hence $E[N(t)] = \int_0^t \lambda(u)du$.

Since as described in Section II, each block representing a dendritic subunit is linear, the voltage response at the soma $v_i(x_i, t)$ due to the activation of the ith dendritic subunit for the input current $i(t)$ can be determined via the Convolution theorem. Hence by exploiting (10), it results

$$v_i(x_i, t) = i(t) \otimes h_i(x_i, t) = \sum_{j=1}^{N(t)} h_i(x_i, t - t_j) \tag{11}$$

where $h_i(x_i, t)$ is the spatiotemporal impulse response of the filter modeling the ith dendritic subunit, characterized in the previous section. To derive the neuron firing probability due to the activation of the ith dendritic subunit in Proposition 1, it is preliminary to stochastically characterize the voltage response $v_i(x_i, t)$, as follows.

From (11), it results that $v_i(x_i, t)$ is a shot-noise process [23]. Hence, by accounting for the generalized Campbell's Theorem [23], we can derive its synthetic characterization, i.e., its mean $\mu_i(x_i, t) \triangleq E[v_i(x_i, t)]$, covariance

function $C_i(x_i,t,\tau) \triangleq E[(v_i(x_i,t)-\mu_i(t))(v_i(x,t-\tau)-\mu_i(t-\tau))]$, and variance $\sigma_i^2(x_i,t) \triangleq E[(v_i(x_i,t)-\mu_i(t))^2]$, as follows:

$$\mu_i(x_i,t) = \int_{-\infty}^{+\infty} h_i(x,t-\tau)\lambda(\tau)d\tau = h_i(x_i,t)\otimes\lambda(t) \tag{12}$$

$$\begin{aligned} C_i(x_i,t,\tau) &= \int_{-\infty}^{+\infty} h_i(x,t-\alpha)h_i(x,t-\tau-\alpha)\lambda(\alpha)d\alpha \\ &= [h_i(x_i,t)h_i(x,t-\tau)]\otimes\lambda(t) \end{aligned} \tag{13}$$

$$\sigma_i^2(x_i,t) = \int_{-\infty}^{+\infty} h_i^2(x,t-\tau)\lambda(\tau)d\tau = h_i^2(x_i,t)\otimes\lambda(t). \tag{14}$$

From (12) to (14), it results that the synthetic characterization of $v_i(x_i,t)$ is function of both the space and the time.

Proposition 1: The probability to excite the neuron past its threshold $v_{\rm th}$, i.e., the firing probability $P_i(x_i,t)$, due to the activation of the ith dendritic subunit is given by

$$P_i(x_i,t) = \int_{v_{\rm th}}^{+\infty}\int_{-\infty}^{+\infty} e^{\int_{-\infty}^{+\infty}\lambda(\alpha)\left[e^{j2\pi\nu h_i(x_i,t-\alpha)}-1\right]d\alpha} e^{-j2\pi\nu\beta}d\nu d\beta \tag{15}$$

with $\lambda(t)$ the rate of the nonhomogeneous Poisson process.

Proof: See Appendix A. ■

Remark 5: From Proposition 1, the firing probability due to the activation of the ith dendritic subunit is the function of: 1) the rate $\lambda(t)$ of the incoming stimulus and 2) the spatiotemporal processing of the dendritic subunit, through its spatiotemporal impulse response $h_i(x_i,t)$.

Since as described in Section II, the dendritic subunit processing is driven by and reflects the functional properties of its collection of synapses [12]–[14] and since the number of synapses is usually high, it could be reasonable to approximate $v_i(x_i,t)$ as a Gaussian process. In such a case, the firing probability derived in Proposition 1 is simplified as follows:

$$P_i(x_i,t) \triangleq P(v_i(x_i,t) > v_{\rm th}) = Q\left(\frac{v_{\rm th}-\mu_i(x_i,t)}{\sigma_i(x_i,t)}\right) \tag{16}$$

with $\mu_i(x_i,t)$ and $\sigma_i(x_i,t)$ given in (12) and (14), respectively.

3) Sufficient Conditions for Null-Response: Here, we derive the conditions on the incoming stimulus impacting on the ith dendritic subunit to induce a null-neuronal response. This is crucial since these conditions provide tools for the nanomachines that can be exploited for avoiding the interference on the surrounding neurons and/or for controlling the neuronal response. To this aim, the following definition is required.

Definition 3: The cutoff frequencies $\{f_j\}_{j=1}^2$ of a filter $F(f)$ are the frequencies at which the filter attenuates the input power by 3 dB[3], i.e., $\{f_j\}_{j=1}^2 : |F(f)|^2 = \frac{1}{2}$.

By substituting the inverse of (7) in the definition of cutoff frequencies, it results that the cutoff frequencies $\{f_{j,i}(x_i)\}_{j=1}^2$ of the ith dendritic subunit $H_i(x_i,f)$ are the frequencies satisfying the following equality:

$$\{f_{j,i}(x_i)\}_{j=1}^2 : r_{a,i}\,|Z_i(f)|\,e^{-2x_i\sqrt{\frac{r_{a,i}}{|Z_i(f)|}}\cos\left(\frac{\angle Z_i(f)}{2}\right)} = 2. \tag{17}$$

Since $H_i(x_i,f)$ varies with x_i, the cutoff frequencies vary with x_i as well. Stemming from (17), the monolateral band of $H_i(x_i,f)$ can be evaluated as $B_i(x_i) \triangleq (f_{1,i}(x_i), f_{2,i}(x_i))$. For the frequency behavior of $H_i(x_i,f)$, the considerations made in Remarks 1 and 2 hold.

Remark 6: Equation (17) discloses the dependence of the cutoff frequencies on both the input impedance $Z_i(f)$ of the ith dendritic subunit and on the location where the stimulus is applied within the ith dendritic subunit through x_i. This is in agreement with the experimental evidences [15], [19].

Remark 7: Different definitions of the cutoff frequencies can be adopted. However, Definition 3 is widely adopted in literature and it does not compromise the following analysis that does not depend on the adopted cutoff frequency definition.

Proposition 2: The firing probability $P_i(x_i,t)$, due to the activation of the ith dendritic subunit, goes to zero when the rate $\lambda(t)$ of the incoming stimulus $i(t)$ has a frequency content that does not belong to the monolateral frequency band $B_{c_i}(x_i) = (f_{1,i}, 2f_{2,i}-f_{1,i})$, with $\{f_{j,i}(x_i)\}_{j=1}^2$ given in (17), whose extension, regardless the definition adopted for the cutoff frequencies, is given by

$$|B_{c_i}(x_i)| = \frac{2e^{2x_i\sqrt{\frac{r_{a,i}}{|Z_i(f_{r,i})|}}\cos\left(\frac{\angle Z_i(f_{r,i})}{2}\right)}}{|Z_i(f_{r,i})|} \cdot \int_0^{+\infty} |Z_i(f)|\,e^{-2x_i\sqrt{\frac{r_{a,i}}{|Z_i(f)|}}\cos\left(\frac{\angle Z_i(f)}{2}\right)}df \tag{18}$$

where $f_{r,i}$ denotes the frequency at which the amplitude response of $h_i(x_i,t)$ assumes its maximum value, i.e., $f_{r,i} : |H_i(x_i,f_{r,i})|^2 = \max_f |H_i(x_i,f)|^2$.

Proof: See Appendix B. ■

Remark 8: From (18), it results that the extension of the frequency band $B_{c_i}(x_i)$ varies with the dendritic membrane impedance, i.e., for example with the density of the voltage-gated ion channels, and/or with the application point of the stimulus on the dendritic subunit through x_i. On the other hand, from Proposition 2, it also results that the incoming burst of spikes controls the activation of the ith dendritic subunit through the temporal patterns of its rate. As a consequence, the number of spikes within the burst does not play a significant role, because adding more spikes to a burst whose rate has a frequency content that does not belong to $B_{c_i}(x_i)$ does not increase the voltage response of the dendritic subunit. This is in agreement with the neuroscience studies [20], [21].

Insight 1: By accounting for Proposition 2 and the above remark, it follows that *the neuronal information is encoded in the stimulus temporal pattern*, i.e., in the time-varying period of the incoming spike train, in agreement with the experimental evidences [15], [19]–[21]. Hence, a stimulus with a certain temporal pattern can activate a certain dendritic subunit and cannot activate another one. Hence, by changing the frequency content

[3]If the filter is a bandpass, the two cutoff frequencies are distinct. If the filter is a low-pass, the two cutoff frequencies degenerate in a single one.

of a burst, a presynaptic neuron selects the dendritic subunits to affect.

Proposition 3: The firing probability $P_i(x_i,t)$, due to the activation of the ith dendritic subunit, goes to zero when the distance x_i between the application point of the incoming stimulus and the soma goes to infinity, even if the incoming rate $\lambda(t)$ has a frequency content belonging to $B_{c_i}(x_i)$ derived in Proposition 2.

Proof: See Appendix C. ■

Insight 2: From Proposition 3, it results that the application point of the incoming stimulus controls the activation of the ith dendritic subunit. Hence, the spatial distribution of the synapses on the postsynaptic neuron determines the dendritic subunits to affect. Hence, through the synapse spatial distribution, a presynaptic neuron selects the dendritic subunits to affect. In this sense, we are allowed to state that *the communication among neurons is spatial-selective*. This is in agreement with the neuroscience studies [12]–[15].

B. Overall Neuronal Response

Here, we characterize the overall neuronal response. To this aim, a preliminary consideration is required. From Proposition 2, it follows that if the input stimulus has a frequency content contained only in the frequency support $B_{c_i}(x_i)$ of one dendritic subunit $h_i(x_i,t)$, the overall neuronal response $v(\bar{x},t)$ coincides with $v_i(x_i,t)$. More in general, if the stimulus has a frequency content contained in the supports of a subset of dendritic subunits $\{h_i(x_i,t)\}_{i\in\mathcal{I}\subseteq\mathcal{D}}$, the cumulative neuronal response $v(\bar{x},t)$ is determined only by the corresponding subset of dendritic subunit responses $\{v_i(x_i,t)\}_{i\in\mathcal{I}\subseteq\mathcal{D}}$. This consideration justifies the following definition.

Definition 4: $H_{\rm eq}(\bar{x},f)$ denotes the spatial-frequency response of the equivalent filter modeling the entire dendritic tree, whose expression is determined by the subset of dendritic subunits activated by the incoming stimulus

$$H_{\rm eq}(\bar{x},f) \triangleq \sum_{i\in\mathcal{I}\subseteq\mathcal{D}} H_i(x_i,f) \tag{19}$$

where $\bar{x}$ is a symbol used to denote the spatial dependence of $H_{\rm eq}(\bar{x},f)$ due to the spatial diversity of the involved dendritic subunits. In the following, we refer to $\bar{x}$ as equivalent distance. The inverse FT of $H_{\rm eq}(\bar{x},f)$ is denoted with $h_{\rm eq}(\bar{x},t)$.

The frequency characterization of $H_{\rm eq}(\bar{x},f)$ follows easily from the analysis developed in the previous section. Specifically, the monolater band of $H_{\rm eq}(\bar{x},f)$ can be evaluated as follows:

$$B_{\rm eq}(\bar{x}) = \bigcup_{i\in\mathcal{I}\subseteq\mathcal{D}} B_i(x_i) \tag{20}$$

with $B_i(x_i)$ given in (17). Definition 3 of the cutoff frequency can be applied also to $H_{\rm eq}(\bar{x},f)$. In particular, if the frequency supports of $\{h_i(x_i,t)\}_{i\in\mathcal{I}\subseteq\mathcal{D}}$ are disjoint, the cutoff frequencies of $H_{\rm eq}(\bar{x},f)$ are the union of the cutoff frequencies of each $H_i(x_i,f)$, i.e., $\{f_{t_{{\rm eq},n}}\}_{n=1}^{2|\mathcal{I}|} = \bigcup_{i\in\mathcal{I}\subseteq\mathcal{D}}\{f_{j,i}\}_{j=1}^{2}$, with $\{f_{j,i}\}_{j=1}^{2}$ given in (17). By accounting for Definition 4, we can now derive the overall neuronal response.

Lemma 1: The overall neuronal response $v(\bar{x},t)$ is a shot-noise process

$$v(\bar{x},t) = \sum_{j=1}^{N(t)} h_{\rm eq}(\bar{x},t-t_j) \tag{21}$$

with spatial time-variant mean, covariance function and variance given by, respectively,

$$\mu(\bar{x},t) \triangleq E[v(\bar{x},t)] = h_{\rm eq}(\bar{x},t)\otimes\lambda(t) \tag{22}$$

$$\begin{aligned} C(\bar{x},t,\tau) &\triangleq E[(v(\bar{x},t)-\mu(\bar{x},t))(v(\bar{x},t-\tau)-\mu(\bar{x},t-\tau))] \\ &= (h_{\rm eq}(\bar{x},t)h_{\rm eq}(\bar{x},t-\tau))\otimes\lambda(t) \end{aligned} \tag{23}$$

$$\sigma^2(\bar{x},t) = C(\bar{x},t,0) = h_{\rm eq}^2(\bar{x},t)\otimes\lambda(t). \tag{24}$$

Proof: See Appendix D. ■

Corollary 1: The probability to excite the neuron past its threshold $v_{\rm th}$, i.e., the firing probability $P(\bar{x},t)$, is given by

$$\begin{aligned} P(\bar{x},t) = \int_{v_{\rm th}}^{+\infty}\int_{-\infty}^{+\infty} & e^{\int_{-\infty}^{+\infty}\lambda(\alpha)\left[e^{j2\pi\nu h_{\rm eq}(\bar{x},t-\alpha)}-1\right]d\alpha} \\ & e^{-j2\pi\nu\beta}d\nu d\beta \end{aligned} \tag{25}$$

with $\lambda(t)$ the rate of the nonhomogeneous Poisson process.

Proof: The proof follows by reasoning as in Proposition 1, since according to Lemma 1, $v(\bar{x},t)$ is a shot-noise process. ■

Remark 9: From Corollary 1, the firing probability is function of the rate of the incoming stimulus, and of the spatiotemporal processing of the dendritic tree through $h_{\rm eq}(\bar{x},t)$.

Since the number of dendrites is usually high, it could be reasonable to approximate $v(\bar{x},t)$ as a Gaussian process. Hence, $P(\bar{x},t)$ derived in Corollary 1 is simplified as follows:

$$P(\bar{x},t) \triangleq P(v(\bar{x},t) > v_{\rm th}) = Q\left(\frac{v_{\rm th}-\mu(\bar{x},t)}{\sigma(\bar{x},t)}\right) \tag{26}$$

where $\mu(\bar{x},t)$ and $\sigma(\bar{x},t)$ are derived in Lemma 1.

Proposition 4: The neuronal firing probability $P(\bar{x},t)$ goes to zero when the rate $\lambda(t)$ of the incoming stimulus $i(t)$ has a frequency content that does not belong to the monolateral frequency band $B_c(\bar{x})$, i.e., to the frequency support of $H_{\rm eq}(\bar{x},f)\otimes H_{\rm eq}(\bar{x},f)$, whose extension, regardless the definition adopted for the cutoff frequencies, is $|B_c(\bar{x})| = 2|B_{\rm eq}(\bar{x})|$, with $B_{\rm eq}(\bar{x})$ given in (20). If the frequency supports of $\{h_i(x_i,t)\}_{i\in\mathcal{I}\subseteq\mathcal{D}}$ are disjoint, the extension of $B_c(\bar{x})$ is

$$|B_c(\bar{x})| = 2\sum_{i\in\mathcal{I}\subseteq\mathcal{D}} |B_i(x_i)| \tag{27}$$

where $|B_i(x_i)| = |B_{c_i}(x_i)|/2$ is given in (18).

Proof: The proof follows by reasoning as in Proposition 2 and by accounting for (20). ■

Remark 10: From Proposition 4, it results that the extension of $B_c(\bar{x})$ varies with the membrane impedances of the activated dendritic subunits and with the equivalent distance $\bar{x}$ that accounts for the overall effect of the application points of the stimulus on the dendritic tree. Moreover, it also results that the incoming burst of spikes controls the neuronal response through

the temporal patterns of its rate. As a consequence, the consideration made for the single dendritic subunit holds also for the overall neuronal response, i.e., the number of spikes within the burst does not play a significant role, because adding more spikes to a burst whose rate has a frequency content that does not belong to $B_c(\bar{x})$ does not increase the neuronal response. This agrees with the neuroscience studies [20], [21].

Insight 3: By accounting for Proposition 4 and the above remark, it follows that a stimulus with a certain temporal pattern can activate a postsynaptic neuron and cannot activate another postsynaptic neuron. Hence by changing the frequency content of a burst, a presynaptic neuron selects the postsynaptic neurons to affect. In this sense, *the communication among neurons is frequency-selective*. This statement is in agreement with the neuroscience studies [15], [20], [21].

Proposition 5: The neuronal firing probability $P(\bar{x}, t)$ goes to zero when the equivalent distance $\bar{x}$ goes to infinity, even if the incoming rate $\lambda(t)$ has a frequency content belonging to $B_c(\bar{x})$ derived in Proposition 4.

Proof: See Appendix E. ■

Note that the equivalent distance $\bar{x}$ goes to infinity when each of the involved distance x_i goes to infinity.

Insight 4: From Proposition 5 and Corollary 1, it results that the application points of the incoming stimulus on the dendritic tree controls the overall neuronal response. Hence, through the spatial distribution of the synapses on the dendritic tree, a presynaptic neuron affects postsynaptic neurons differently.

IV. Validation of the Theoretical Results

Here, we validate the theoretical results through simulations. Specifically, we use the realistic experimentally reconstructed rat neuron morphology "P20-DEV139" downloaded from NeuroMorpho.org archive as done in [15]. The neuron morphology is shown in Fig. 3. The considered cell exhibits an archetypical multipolar morphology, and the membrane impedance for the arbitrary dendritic subunit is equal to [4]

$$|Z_i(\omega)| = \frac{\tau}{C}\sqrt{\frac{1+\tau^2\omega^2}{(a+b-\tau^2\omega^2)^2+\tau^2\omega^2(1+a)^2}} \tag{28}$$

$$\angle Z_i(\omega) = \tan^{-1}\left(\tau\omega\frac{b-(1+\tau^2\omega^2)}{b+a(1+\tau^2\omega^2)}\right) \tag{29}$$

where $\omega = 2\pi f$. By choosing $a = \{2,\ 0.2\}$ and $b = \{2,\ 1.1\}$ as in [4], we obtain the impedances of the two dendritic subunits shown in Fig. 3, which act in frequency as pass-band as depicted in Fig. 4.

In Fig. 4, the normalized modulus of the spatial-frequency responses $\{H_i(x_i, f)\}_{i=1}^2$ are plotted as function of the frequency and of the dendritic lengths x_i (whose values are available on NeuroMorpho.org for the considered neuron morphology). The red lines in the figure represent the profile of the modulus of the membrane impedances $|Z_i(f)|$ of the two dendritic subunits, with the arrows indicating the trend of increasing x_i. In agreement with Remark 2, when the stimulus is injected near the soma, the resonance frequency of $\{H_i(x_i, f)\}_{i=1}^2$ is mostly that of the input impedance. When x_i increases, the resonance frequency of $\{H_i(x_i, f)\}_{i=1}^2$ becomes more influenced by the resonance frequency of the frequency-dependent space constant $\gamma(f)$, as observed in [19].

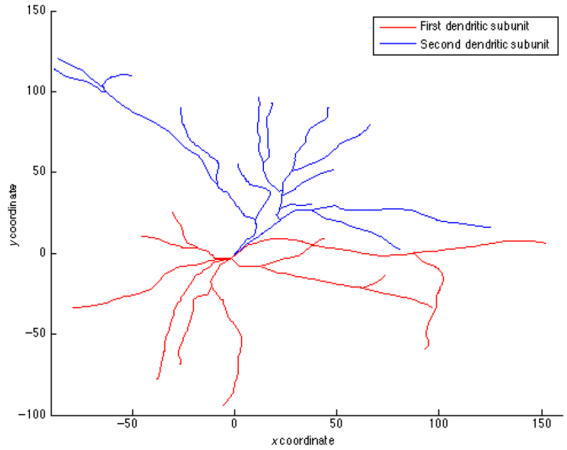

Fig. 3. Multipolar rat neuron morphology P20-DEV139 with a dendritic tree composed by two dendritic subunits. Coordinates are expressed in μm.

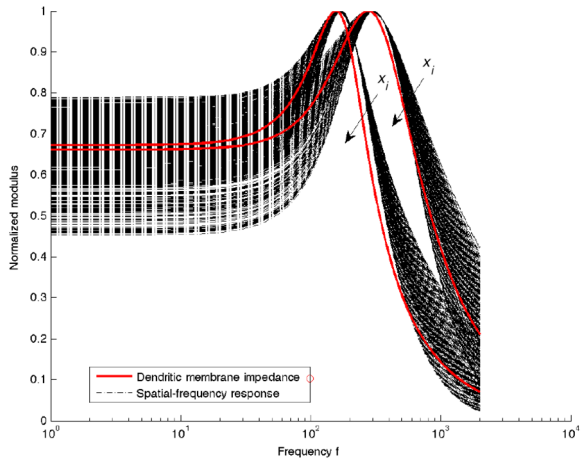

Fig. 4. Normalized spatial-frequency response modulus $|H_i(x_i, f)|$ as function of the frequency f for different dendritic subunit lengths x_i.

In Fig. 5, we focus on the first dendritic subunit by plotting the normalized modulus $|H_1(x_1, f)|$ of the spatial-frequency response as function of the frequency and of the dendritic length x_1. In agreement with the experimental evidences, the attenuation increases as the distance x_1 between the stimulus injection point and the soma increases.

The resonance frequencies observed in Fig. 4 have been reported in Fig. 6 to underline their spatial profile. It is worthwhile to note that the range of the resonance frequencies, approximately [160, 305] Hz, agrees with the results in [15].

In Fig. 7 and 8, we report the spatial map of the attenuations experienced by a stimulus injected at coordinates (x, y) through the dendrites for two different values of the incoming stimulus frequency, i.e., 100 and 400 Hz. In agreement with the analysis developed in Section III, the attenuation increases as the distance between the stimulus injection point and the soma increases. Furthermore, we observe that the attenuation experienced by a stimulus injected at a given distance in the first dendritic subunit can differ from the attenuation experienced

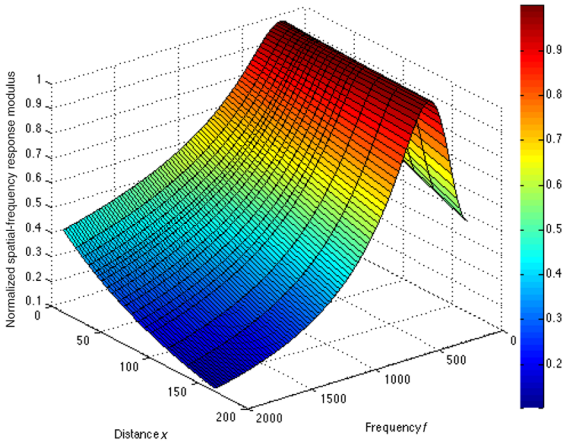

Fig. 5. Normalized spatial-frequency response modulus $|H_1(x_1, f)|$ as function of the frequency f and length x for the first dendritic subunit.

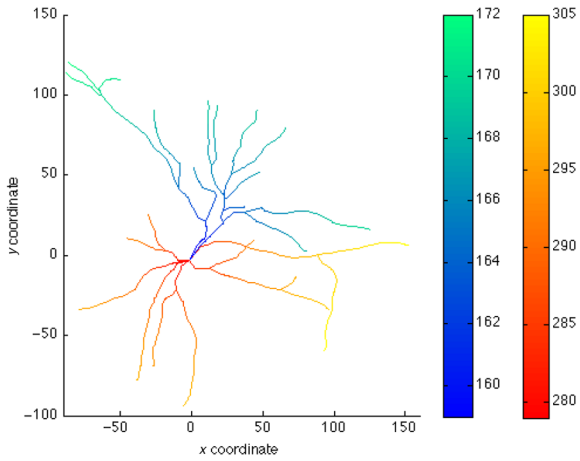

Fig. 6. Spatial map of the resonance frequencies.

by a stimulus injected at the same distance in the second dendritic subunit. This phenomenon accounts for the nonuniform electrical properties of the dendritic tree, and it agrees with the experimental evidences. Finally, we note that the two dendritic subunits exhibit different frequency preferences for the considered values. Specifically, the attenuation of the first subunit is roughly the same for the two considered values, whereas the attenuation of the second subunit increases with the distance faster at 400 Hz than at 100 Hz.

In Figs. 9 and 10, we report the spatial map of the normalized delays experienced by a stimulus injected at coordinates (x, y) through the dendrites for two different values of the incoming stimulus frequency, i.e., 100 Hz and 400 Hz. In agreement with the developed theoretical analysis, the delays increase as the distance between the stimulus injection point and the soma increases. Furthermore, we note that the delays experienced by a stimulus injected at the first subunit differ significantly from those experienced by a stimulus injected at the second subunit. Specifically, the delays experienced at the first subunit are shorter than those experienced at the second subunit at 100 Hz, whereas the opposite holds at 400 Hz. This result clearly reveals the huge dendritic processing power.

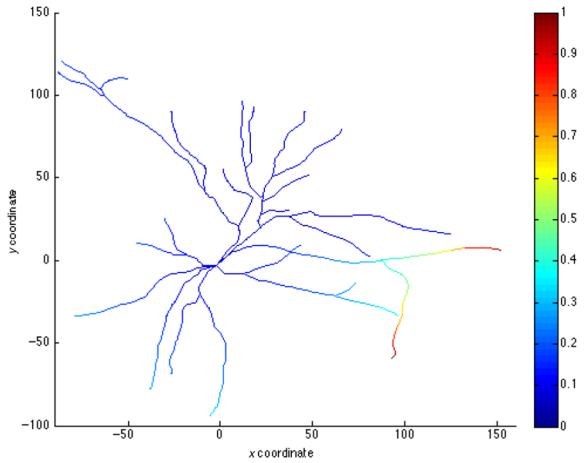

Fig. 7. Spatial map of the attenuations experienced by a stimulus at frequency 100 Hz injected at (x, y).

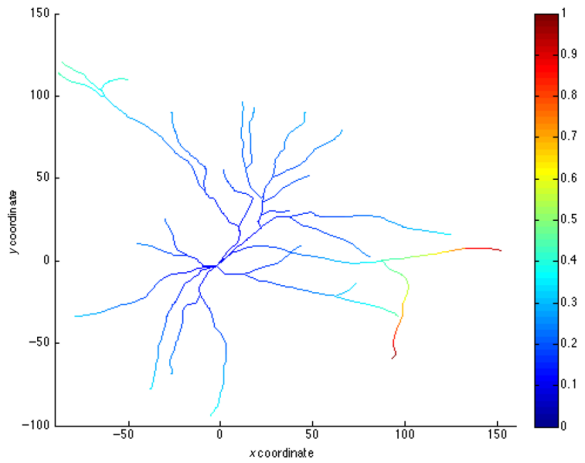

Fig. 8. Spatial map of the attenuations experienced by a stimulus at frequency 400 Hz injected at (x, y).

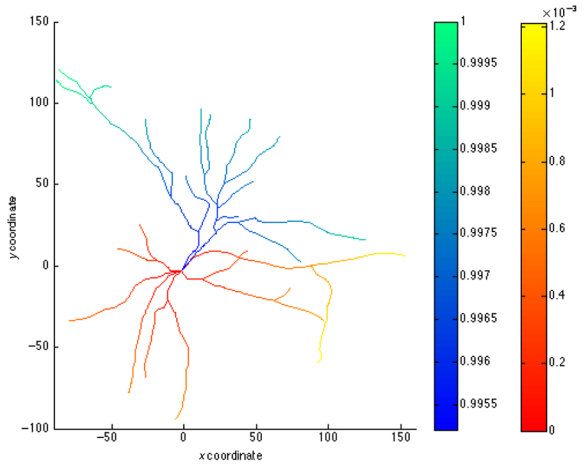

Fig. 9. Spatial map of the normalized delays experienced by a stimulus at frequency 100 Hz injected at (x, y).

To validate the analysis about the spatial-frequency selectivity of the neuronal communications, we probe the considered neuron with an input current that sweeps through the frequencies belonging to the interval [1,1500] Hz over the time, known

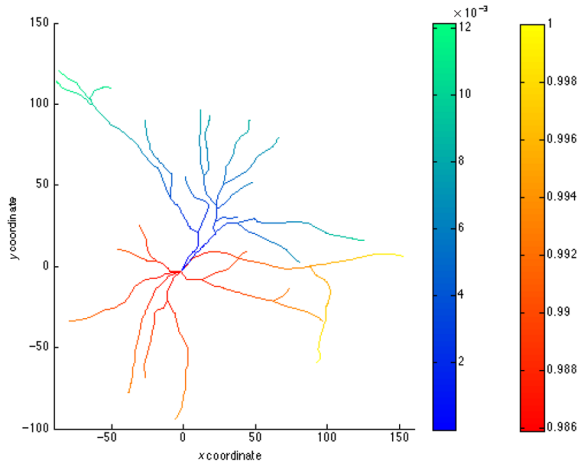

Fig. 10. Spatial map of the normalized delays experienced by a stimulus at frequency 400 Hz injected at (x, y).

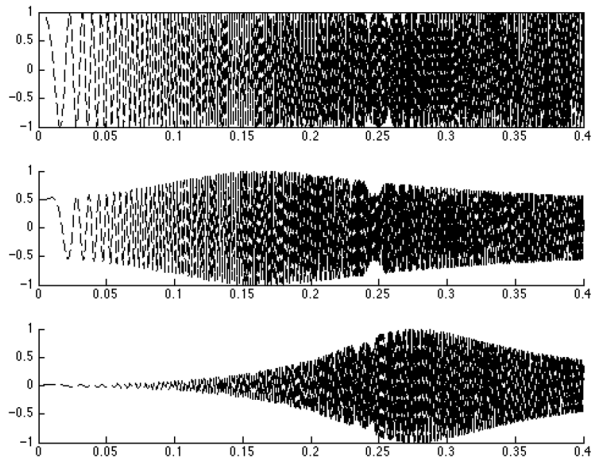

Fig. 11. Frequency–selectivity: first dendritic subunit response (second plot) and second dendritic subunit response (third plot) for a ZAP (first plot) stimulus injected at coordinates $(4.1, 6.02)$ and $(92.84, -59.23)$, respectively.

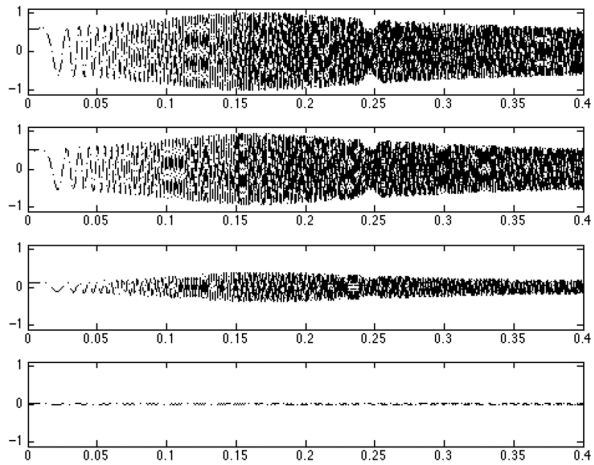

Fig. 12. Spatial–selectivity: dendritic subunit length impacts on the neuronal response for the first subunit at length $x_1 = 1$ (first plot), $x_1 = 10$ (second plot), $x_1 = 100$ (third plot), and $x_1 = 1000$ (fourth plot).

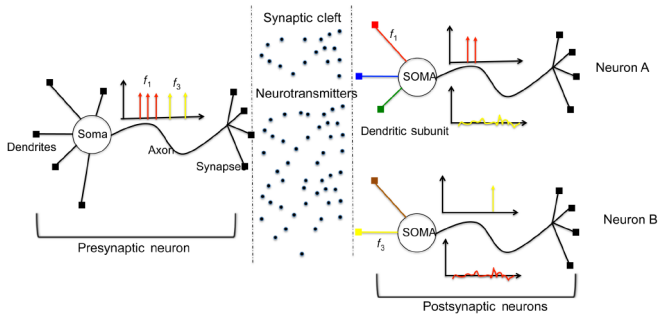

Fig. 13. Spatial-frequency selectivity: an incoming stimulus with multiplexed interspike frequency $f_1 + f_2$ activates both the dendritic subunits denoted with the red and the yellow colors of two distinct postsynaptic neurons A and B, without any cross interference with each other.

as ZAP current, as widely done in literature [4]. Specifically, in Fig. 11, we report the two dendritic subunit responses as function of the time for the ZAP injected at coordinates $(4.1, 6.02)$ and $(92.84, -59.23)$, respectively. We note that the first dendritic subunit with resonance frequency $f = 307$ Hz attenuates the frequencies outside its 3 dB band, i.e., not belonging to the range $[1, 850]$ Hz. Vice versa, the second dendritic subunit with resonance frequency $f = 518$ attenuates all the frequencies not in $[388, 720]$ Hz, which roughly corresponds to its 3 dB band. The results validate the conducted analysis. In fact, the activation of the dendritic subunits depends on the temporal patterns of the stimulus, i.e., the neuronal information is contained in the timing of the stimulus (Propositions 2 and 4). Hence, a stimulus with a certain temporal pattern can activate certain dendritic subunits and cannot activate another ones.

Finally, Fig. 12 shows the response of the first dendritic unit as function of the time for different values of the distance between the application point of the ZAP current and the soma, i.e., $x_1 = \{1, 10, 100, 1000\}$. We note that the dendritic response decreases when the distance increases in agreement with the theoretical analysis (Propositions 3 and 5). For $x_1 = 1000$, the response is roughly null.

V. Discussion

In agreement with experimental evidences [12]–[15], [20], [21], the conducted theoretical analysis reveals the following.

1) *The neuronal information is encoded in the stimulus temporal pattern*. Hence, a stimulus with a certain temporal pattern can activate a postsynaptic neuron and cannot activate another postsynaptic neuron, as depicted in Fig. 13. In this sense, the *communication among neurons is frequency-selective*.
2) The spatial distribution of the dendritic subunits controls the overall neuronal response and the expressed frequency preference. Hence, the neuronal response changes by changing the application point of a stimulus within the dendritic tree, as depicted in Fig. 13. In this sense, *the communication among neurons is spatial-selective*.

The implications of the aforementioned results are crucial for the development of future IoNT applications based on the deployment of nanomachines inside the nervous system, e.g., radically new medical diagnosis and treatment techniques. In fact, the spatial-frequency selectivity of the communications

among neurons can be exploited for the implementation of novel communication techniques between the nanomachines and/or between nanomachines and natural neurons, along with controlling strategies of network topology and connectivity. Specifically, a nanomachine could force a neuronal response by properly selecting the frequency content of its emitted signal. Moreover, a nanomachine could limit the possible interference generated on the normal neuronal activities by exploiting the spatial-frequency selectivity of the surrounding neurons. In other words, if the communications among nanomachines use frequencies that do not activate the surrounding neurons, no interference is generated.

We also underline that to fully realize the IoNT paradigm, the nanomachines deployed inside the nervous system have to be interconnected to the Internet. To this aim, an architecture to interface the nanonetwork deployed inside the nervous system and the external environment, ultimately Internet, is required. Some interesting results in this research direction have been drawn in [5], where the authors propose an ultra-miniature as well as extremely compliant system for brain–machine interfaces. However, further research is required before a truly functional interface between a nanomachines deployed inside the nervous system and the external environment is realized.

VI. Conclusion

In this paper, we proposed a receiver model for capturing the behavior of biological neurons, by accounting for two peculiar features of the dendritic biophysics: 1) the compartmentalization at the level of individual dendritic subunits of the neuronal processes and 2) the location-dependent preference for different frequencies. Specifically, we have modeled a dendritic tree as a spatiotemporal filter bank, where each filter models the behavior in both space and time of a dendritic subunit. Our theoretical analysis reveled that: 1) the neuronal information is encoded in the stimulus temporal pattern, i.e., the communication among neurons is *frequency-selective* and 2) the spatial distribution of the synapses on the postsynaptic neuron determine the dendritic subunits to affect, i.e., the communication among neurons is *spatial-selective*.

Appendix A
Proof of Proposition 1

The firing probability due to the activation of the ith dendritic subunit is given by

$$P_i(x_i,t) \triangleq P(v_i(x_i,t) > v_{\rm th}) = \int_{v_{\rm th}}^{+\infty} f_{v_i}(x_i,t;\beta)d\beta \quad (30)$$

where $f_{v_i}(x_i,t;v)$ denotes the pdf of the random process $v_i(x_i,t)$. Using the FT relation between the Characteristic Function (CF) and the pdf of a random variable [23], it results $f_{v_i}(x_i,t;v) = \int_{-\infty}^{+\infty} \Phi(x_i,\nu)e^{-j2\pi\nu v}d\nu$, where the spatial CF $\Phi(x_i,\nu)$ for the nonhomogeneous shot-noise process $v_i(x_i,t)$ can be obtained by generalizing the CF for a spatial constant nonhomogeneous shot-noise process [23] as follows:

$$\Phi(x_i,\nu) = e^{\int_{-\infty}^{+\infty}\lambda(\alpha)\left[e^{j2\pi\nu h_i(x_i,t-\alpha)}-1\right]d\alpha}. \quad (31)$$

By substituting (31) in (30), the proof follows.

Appendix B
Proof of Proposition 2

The extension of the monolateral band of $h_i(x_i,t)$ can be calculated as follows:

$$E_i(x_i) = \int_0^{+\infty} \left|\frac{H_i(x_i,f)}{H_i(x_i,f_{r,i})}\right|^2 df \quad (32)$$

By substituting (7) in (32), after easy algebraic manipulations, one obtains

$$E_i(x_i) = \frac{e^{2x_i\sqrt{\frac{r_{a,i}}{|Z_i(f_{r,i})|}}\cos\left(\frac{\angle Z_i(f_{r,i})}{2}\right)}}{|Z_i(f_{r,i})|} \int_0^{+\infty} |Z_i(f)|\, e^{-2x_i\sqrt{\frac{r_{a,i}}{|Z_i(f)|}}\cos\left(\frac{\angle Z_i(f)}{2}\right)} df. \quad (33)$$

From (14), it results that the FT $\Sigma(x_i,f)$ of $\sigma^2_{v_i}(x_i,t)$ is

$$\Sigma(x_i,f) = \left(H_i(x_i,f)\otimes H_i(x_i,f)\right)\Lambda(f). \quad (34)$$

From (34) and by accounting for (12), it results that when the frequency support of $\lambda(t)$ is not contained in the frequency support of $H_i(x_i,f)\otimes H_i(x_i,f)$, $v_i(x_i,t)$ is null identically. In fact, its variance and mean are null identically, hence $v_i(x_i,t)$ assumes with probability one its expected value, i.e., zero. Stemming from this and by accounting for the elementary properties of the convolution operator, the proof follows since the frequency support of $H_i(x_i,f)\otimes H_i(x_i,f)$ is $B_{c_i}(x_i) = (f_{1,i}, 2f_{2,i} - f_{1,i})$, whose extension is $2E_i(x_i)$, with $E_i(x_i)$ given in (33) and $\{f_{j,i}\}_{j=1}^2$ given in (17).

Appendix C
Proof of Proposition 3

By accounting for (6), it results

$$\lim_{x_i\to\infty} |H_i(x_i,f)| = 0. \quad (35)$$

Hence, even if the frequency content of $\lambda(t)$ is contained in the frequency support of $H_i(x_i,f)\otimes H_i(x_i,f)$, i.e., in B_{c_i}, the response of the ith dendritic subunit is null identically.

Appendix D
Proof of Lemma 1

In literature, it is widely adopted a linear model for the interaction among distinct dendritic subunits [12]. Hence, $v(\bar{x},t) = \sum_{i\in\mathcal{I}\subseteq\mathcal{D}} v_i(x_i,t)$. By exploiting (11) and (19), it results

$$v(\bar{x},t) = \sum_{i\in\mathcal{I}\subseteq\mathcal{D}} i(t)\otimes h_i(x_i,t) = i(t)\otimes h_{\rm eq}(\bar{x},t) = \sum_{j=1}^{N(t)} h_{\rm eq}(\bar{x},t-t_j). \quad (36)$$

Hence, $v(\bar{x},t)$ is a shot-noise process [23], whose characterization can be obtained similar to $v_i(x_i,t)$ by applying the generalized Campbell's Theorem. As a consequence, (22)–(24) are immediately obtained.

APPENDIX E
PROOF OF PROPOSITION 5

By accounting for (19), it results

$$\begin{aligned}\lim_{\bar{x}\to\infty}|H_{\rm eq}(\bar{x},f)| &= \lim_{\bar{x}\to\infty}|\sum_{i\in\mathcal{I}\subseteq\mathcal{D}}H_i(x_i,f)| \\ &\leq \sum_{i\in\mathcal{I}\subseteq\mathcal{D}}\lim_{\bar{x}\to\infty}|H_i(x_i,f)| \\ &= \sum_{i\in\mathcal{I}\subseteq\mathcal{D}}\lim_{x_i\to\infty}|H_i(x_i,f)| = 0. \qquad (37)\end{aligned}$$

Hence, even if the frequency content of $\lambda(t)$ is contained in the frequency support of $H_{\rm eq}(\bar{x},f)\otimes H_{\rm eq}(\bar{x},f)$, i.e., in B_c, the neuronal response is null identically.

REFERENCES

[1] I. Akyildiz and J. Jornet, "The Internet of Nano-Things," *IEEE Wireless Commun.*, vol. 17, no. 6, pp. 58–63, Dec. 2010.

[2] I. F. Akyildiz, J. M. Jornet, and M. Pierobon, "Nanonetworks: A new frontier in communications," *ACM Commun.*, vol. 54, no. 11, pp. 84–89, Nov. 2011.

[3] F. Mesiti and I. Balasingham, "Nanomachine-to-neuron communication interfaces for neuronal stimulation at nanoscale," *IEEE J. Sel. Areas Commun.*, vol. 31, no. 12, pp. 695–704, Dec. 2013.

[4] M. Veletic, P. A. Floor, and I. Balasingham, "From nano-scale neural excitability to long term synaptic modification," in *Proc. ACM NanoCom*, May 2014, pp. 1–8.

[5] D. Seo, J. M. Carmena, J. M. Rabaey, E. Alon, and M. M. Maharbiz, "Neural dust: An ultrasonic, low power solution for chronic brain-machine interfaces," arxiv, Jul. 2013, arxiv.org/abs/1307.2196.

[6] J. Suzuki, S. Balasubramaniam, S. Pautot, V. D. P. Meza, and Y. Koucheryavy, "A service-oriented architecture for body area nanonetworks with neuron-based molecular communication," *Mobile Netw. Appl.*, vol. 19, no. 6, pp. 707–717, Nov. 2014.

[7] T. Denison, M. Morris, and F. Sun, "Building a bionic nervous system," *IEEE Spectr.*, vol. 52, no. 2, pp. 32–39, Feb. 2015.

[8] D. Malak and O. Akan, "Communication theoretical understanding of intra-body nervous nanonetworks," *IEEE Commun. Mag.*, vol. 52, no. 4, pp. 129–135, Apr. 2014.

[9] I. Segev and M. London, "Untangling dendrites with quantitative models," *Science*, vol. 290, no. 5492, pp. 744–750, 2000.

[10] W. E. Kaufmann and H. W. Moser, "Dendritic anomalies in disorders associated with mental retardation," *Cerebral Cortex*, vol. 10, no. 10, pp. 981–991, 2000.

[11] B. H. Anderton *et al.*, "Dendritic changes in Alzheimer's disease and factors that may underlie these changes," *Prog. Neurobiol.*, vol. 55, no. 6, pp. 595–609, 1998.

[12] T. Branco and M. Hausser, "The single dendritic branch as a fundamental functional unit in the nervous system," *Current Opinion Neurobiol.*, vol. 20, no. 4, pp. 494–502, 2010.

[13] A. Polsky, B. Mel, and J. Schiller, "Computational subunits in thin dendrites of pyramidal cells," *Nat. Neurosci.*, vol. 9, no. 3, pp. 206–221, Mar. 2008.

[14] C. Koch, T. Poggio, and V. Torres, "Retinal ganglion cells: A functional interpretation of dendritic morphology," *Philos. Trans. R. Soc. Lond. B, Biol. Sci.*, vol. 298, no. 1090, pp. 227–263, 1982.

[15] J. Laudanski, B. Torben-Nielsen, I. Segev, and S. Shamma, "Spatially distributed dendritic resonance selectively filters synaptic input," *PLoS Comput. Biol.*, vol. 10, no. 8, pp. 1–10, Aug. 2014.

[16] E. Zhuchkova, M. Remme, and S. Schreiber, "Subthreshold resonance and membrane potential oscillations in a neuron with nonuniform active dendritic properties," in *The Computing Dendrite*. New York, NY, USA: Springer, 2014, vol. 11, ch. 20, pp. 331–346.

[17] I. Segev, "Cable and compartmental models of dendritic trees," in *The Book of Genesis: Exploring Realistic Neural Models with the General NEural SImulation System*, J. M. Bower and D. Beeman, Eds., Internet ed. New York, NY, USA: Springer, 2003, ch. 5.

[18] A. Schoen, A. Salehiomran, M. E. Larkum, and E. P. Cook, "A compartmental model of linear resonance and signal transfer in dendrites," *Neural Comput.*, vol. 24, no. 12, pp. 3126–3144, Dec. 2012.

[19] C. Koch, "Cable theory in neurons with active, linearized membranes," *Biol. Cybern.*, vol. 50, no. 1, pp. 15–33, 1984.

[20] E. M. Izhikevich and E. C. W. N. S. Desai, "Bursts as a unit of neural information: Selective communication via resonance," *Trends Neurosci.*, vol. 26, no. 3, pp. 161–167, 2003.

[21] B. Hutcheon and Y. Yarom, "Resonance, oscillation and the intrinsic frequency preferences of neurons," *Trends Neurosci.*, vol. 23, no. 5, pp. 216–222, 2000.

[22] C. Koch and T. Poggio, "A simple algorithm for solving the cable equation in dendritic trees of arbitrary geometry," *J. Neurosci. Methods*, vol. 12, no. 4, pp. 303–315, 1985.

[23] A. Papoulis, *Probability, Random Variables, and Stochastic Processes*. New York, NY, USA: McGraw-Hill, 1984.

Angela Sara Cacciapuoti (M'10) received the Dr. Eng. degree (*summa cum laude*) in telecommunications and Ph.D. degree in electronic and telecommunications engineering from the University of Naples Federico II, Naples, Italy, in 2005 and 2009, respectively.

She is currently an Assistant Professor with the DIETI Department, University of Naples Federico II. From 2010 to 2011, she was with the Broadband Wireless Networking Laboratory, Georgia Institute of Technology, Atlanta, GA, USA, as a Visiting Researcher. In 2011, she was also with the NaNoNetworking Center in Catalunya (N3Cat), Universitat Politècnica de Catalunya (UPC), as a Visiting Researcher. She is an Area Editor of *Computer Networks*. Her research interests include cognitive radio networks and nanonetworks.

Marcello Caleffi (GSM'06–M'12) received the Dr. Eng. degree (*summa cum laude*) in computer science from the University of Lecce, Lecce, Italy, in 2005, and the Ph.D. degree in electronic and telecommunications engineering from the University of Naples Federico II, Naples, Italy, in 2009.

He is currently an Assistant Professor with the DIETI Department, University of Naples Federico II. From 2010 to 2011, he was with the Broadband Wireless Networking Laboratory, Georgia Institute of Technology, Atlanta, GA, USA, as a Visiting Researcher. In 2011, he was also with the NaNoNetworking Center in Catalunya (N3Cat), Universitat Politècnica de Catalunya (UPC), Barcelona, Spain, as a Visiting Researcher. He serves as Area Editor with the *Elsevier Ad Hoc Networks*. His research interests include cognitive radio networks and biological networks.